photochem

Article

Efficient Access of Phenyl-Spaced 5,5′-Bridged Dinuclear Ruthenium Metal Complexes and the Effect of Dynamic Ligand Exchange on Catalysis

Martin Lämmle, Steffen Volk, Madelyn Klinkerman [ID], Marius Müßler, Alexander K. Mengele [ID] and Sven Rau *[ID]

Institute of Inorganic Chemistry I, Ulm University, Albert-Einstein-Allee 11, 89081 Ulm, Germany
* Correspondence: sven.rau@uni-ulm.de

Abstract: Herein, we present the synthesis, characterization, and light-driven hydrogen evolution activity of two dinuclear Ru-Pt complexes, **Rup(ph)pPtX$_2$** (X = Cl, I), comprising a new phenyl-spaced 5,5′-bis-phenanthroline **p(ph)p** bridging ligand. The two complexes only differ in the nature of the halide ligand at the catalytic center. Structural, photophysical, electrochemical, as well as photochemical characterization techniques revealed that the variations of single components of the intramolecular system provide a strong influence on the stability even in non-catalytic conditions. Interestingly, varying electron density at the catalytic center, mainly influenced by the coordinating halide at the catalytic center, as shown by ^{195}Pt NMR spectroscopy, strongly influences the photocatalytic efficiency. Furthermore, intensive investigations on the potential catalytic mechanism showed that small structural variations (e.g., halide exchange) not only affect catalytic activity but can also switch the main catalytic mechanism from an initially molecular one to a fully heterogeneous, colloid-driven hydrogen evolution.

Keywords: ruthenium; photocatalysis; hydrogen; colloids; ligands

1. Introduction

In order to prevent high economic and ecological damage, global warming has to be capped at about 1.5 °C compared to pre-industrial times [1–3]. To overcome the main problem of renewable energies, i.e., they are not continuously available, storage capacities for the harvested energy have to be built up. These can either consist of physical storage (e.g., water-pumped storage power plants), electrical storage (e.g., batteries), or chemical storage (e.g., synthetic liquid fuels or hydrogen). As a cascade of multiple transformation steps from light energy into chemical energy is inherently connected with a decreasing overall efficiency, the direct usage of photonic energy for the generation of energy-rich chemical compounds seems to be promising.

The development of photocatalytically active systems for hydrogen evolution can rely on inter- (multi-component) or intramolecular (single-component) systems. In intermolecular systems, the electron is transferred directly or via electron relay from the photosensitizer (e.g., [Ru(bpy)$_3$]$^{2+}$ [4]) to the catalytic center, i.e., both functionalities are represented by individual molecular species [5,6]. However, a direct connection of the photosensitizer (e.g., [Ru(bpy)$_3$]$^{2+}$ [7,8]) via an organic bridging ligand with the catalytic center (e.g., Rh [9], Pt [7,10–13], Pd [7], Co [14–16], . . .) needs no separated electron relay. Furthermore, intramolecular systems help to understand the catalytic mechanism, as detailed structure relationships can be obtained [17–19].

Rau et al. described earlier that [(tbbpy)$_2$Ru(tpphz)PtCl$_2$/I$_2$](PF$_6$)$_2$ (tbbpy = 4,4′-di-*tert*-butyl-2,2′-bipyridine; tpphz = tetrapyrido [3,2-a:2′,3′-c:3′′,2′′-h:2′′′,3′′′-j]phenazine), as well as [(tbbpy)$_2$Ru(tpphz)PdCl$_2$](PF$_6$)$_2$, are capable of converting light energy into chemical bond energy (see Figure 1) via a photoinduced intramolecular electron transfer

to the catalytic center (CC), where hydrogen is finally evolved [7,12]. However, the instability of the intramolecular systems plays a crucial role in preventing high efficiency and reliable long-term performance. In this context, Hammarström et al. described earlier that Pd systems tend to form catalytically active Pd colloids using the non-conjugated [(bpy)$_2$Ru(DMB)PdCl$_2$]$^{2+}$ (DMB = 4′,4‴-((2,5-dimethoxy-1,3-phenylene)bis(ethane-2,1-diyl))bis(4-methyl-2,2′-bipyridine) complex [20]. High chemical and photochemical stability combined with the superior photocatalytic activity of [(tbbpy)$_2$Ru(tpphz)PtI$_2$](PF$_6$)$_2$ allowed for detailed investigations into its behavior as a molecular photocatalyst. They revealed a so-far unprecedented ability for molecular repair. Stability, as well as the accessibility of repair, correlates with the utilized tpphz bridging ligand [7,12,21]. Further investigations into this interesting behavior require synthetic access to new bridging ligands, as they have a strong influence on the stabilization of the catalytic center and the stability of the organic scaffold of the bridging ligand itself [18,21].

Previous work:
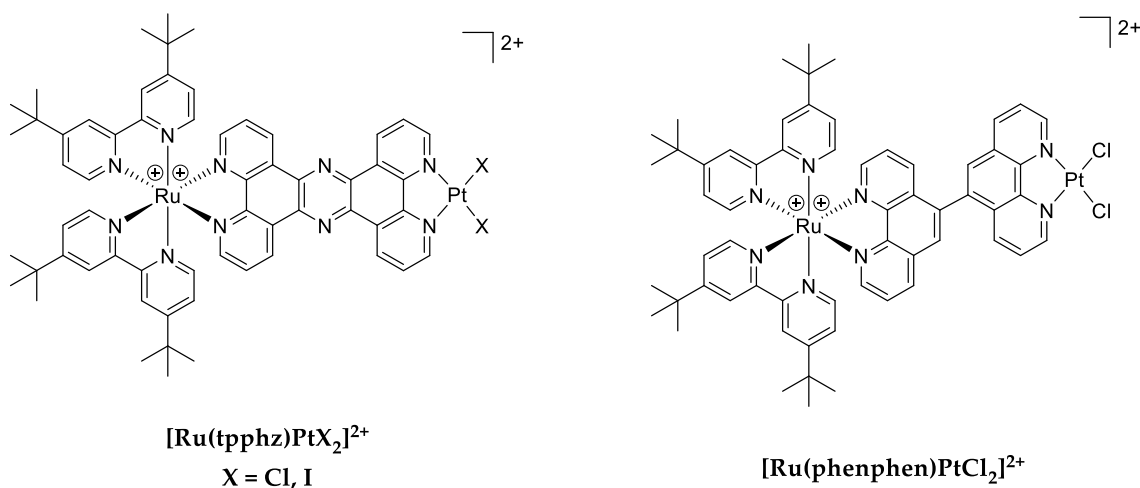
This work:

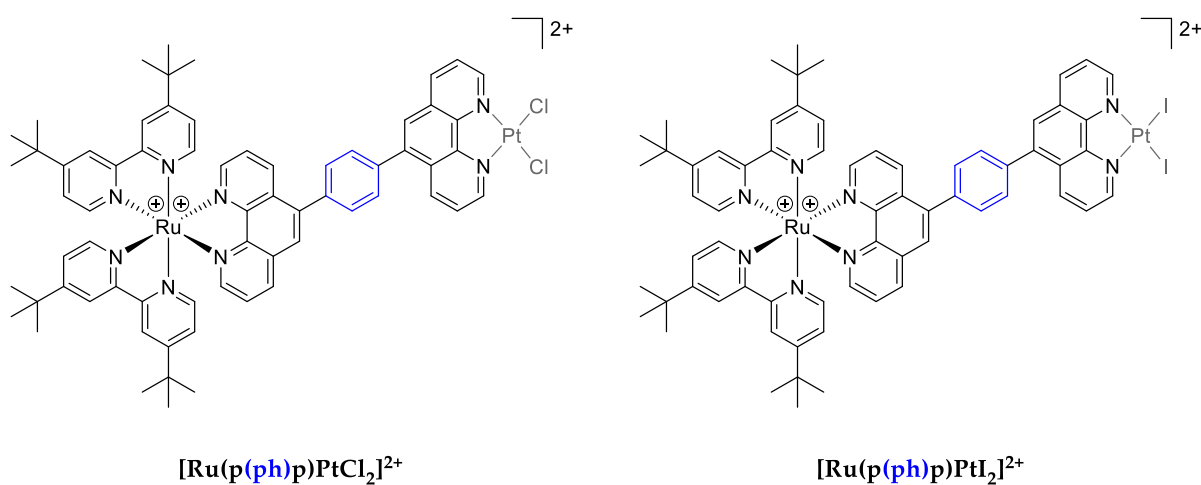**Figure 1.** Overview of previous work on directly linked 5,5′-bis-1,10-phenanthroline phenphen systems [Ru(tpphz)PtX$_2$]$^{2+}$ (left) and [Ru(phenphen)PtCl$_2$]$^{2+}$ (right) and the herein investigated phenyl-spaced **p(ph)p**-system [Ru(p(ph)p)PtX$_2$]$^{2+}$ (**p(ph)p** = 1,4-bis(1,10-phenanthroline-5-yl)benzene) in this study.

As Campagna et al. and Rau et al. described earlier, a directly C-C-linked 5,5′-bis-1,10-phenanthroline ligand (phenphen) can be used as a bridging ligand (BL) for dinuclear, intramolecular catalysts, e.g., [(tbbpy)$_2$Ru(phenphen)PtCl$_2$]$^{2+}$ (Ru(phenphen)PtCl$_2$) [8,22]. Since the phenphen BL architecture provides a nearly perpendicular orientation of the two 1,10-phenanthroline spheres, no excited-state interaction between PS and CC, contrary to the planar tpphz system, can occur. Interestingly, the phenphen-based system was still active in light-driven hydrogen evolution. However, hydrogen evolution stopped after 120 min due to the instability of the Pt center and concomitant particle formation. Previous studies by our group showed that the nature of a spacer (e.g., triazole or alkyne) between the two phenanthrolines of a bis-phenanthroline-based BL has a significant influence on the catalytic activity for the light-driven reduction of NAD$^+$ to NADH [18]. In these dinuclear RuRh photocatalysts, the alkyne spacer initially enabled ca. 6-fold higher catalytic activity compared to the triazole-based system. However, the alkyne-bridged Ru-Rh system was easily hydrogenated at the triple-bond, leading to the loss of its high catalytic activity [18]. As hydrogen evolution reactions (HERs) take place under reductive conditions, the introduction of a chemically stable spacer is crucial for overall efficiency and long-term performance [21].

In this work, we present a series of mono- and dinuclear Ru polypyridyl complexes connected to the catalytic center via the phenyl-spaced **p(ph)p** bridging ligand (p(ph)p = 1,4-bis(1,10-phenanthrolin-5-yl)benzene). This bridging ligand provides a large distance between the two metal binding sites and has the potential to reduce sterical strain as the linking unit compared to the phenphen ligand. Contrary to the studies by Higuchi et al. who utilized the **p(ph)p** ligand to construct Ruthenium-based multimetallic polymers for catalytic transfer hydrogenations, we focus on mono- and dinuclear Ru-compounds [23]. We therefore synthesized the **p(ph)p** ligand followed by the mononuclear [(tbbpy)$_2$Ru(p(ph)p)](PF$_6$)$_2$ complex (**Rup(ph)p**), finally serving as the precursor for the homodinuclear complex [(tbbpy)$_2$Ru(p(ph)p)Ru(tbbpy)$_2$](PF$_6$)$_4$ (**Rup(ph)pRu**), as well as the two heterodinuclear complexes [(tbbpy)$_2$Ru(p(ph)p)PtX$_2$](PF$_6$)$_2$ (**Rup(ph)pPtX$_2$** (X = Cl or I), see Figure 1). All complexes were investigated in detail on their structural, photophysical, photochemical and electrochemical properties. The dinuclear systems, **Rup(ph)pPtCl$_2$/I$_2$**, were also tested for catalytic activity in light-driven hydrogen evolution.

2. Materials and Methods

5-Bromo-1,10-phenanthroline [24], [Ru(tbbpy)$_2$Cl$_2$] [25], and [Pt(DMSO)$_2$Cl$_2$] [26] were synthesized according to the literature's procedures. 1,4-bis(4,4,4,4-tetramethyl-1,2,3-dioxoborolan-2-yl)benzene, Pd(PPh$_3$)$_2$Cl$_2$, NH$_4$PF$_6$, deuterated solvents, solvents for absorption and emission studies, dry DMSO, and acetonitrile were purchased from Sigma Aldrich or Carl Roth®. K$_2$CO$_3$ was purchased from ABCR. All other technical-grade solvents were purchased by VWR. All chemicals were used without further purification. All solvents were distilled before use. All ^{1}H NMR signals were assigned using 2D-NMR techniques.

2.1. Steady-State UV/vis Absorption Spectroscopy

Steady-state absorption spectra were recorded on a JASCO V-670 at room temperature using a slit width of 1 nm and a scan rate of 400 nm/min. All spectra were recorded using a quartz glass cuvette of 10 × 10 mm and Roth® ROTISOLV® UV/IR-grade solvents. For absorption spectroscopy, the absorbance was typically kept below 1 within the investigated wavelength range from 250 nm to 900 nm. This is obtained with Ru complex concentrations lower than 10^{-5} M.

2.2. Steady-State Emission Spectroscopy

Steady-state emission spectra were recorded on a JASCO FP-8500 Fluorescence spectrometer (aerated and deaerated measurements). The studies were performed in 10 × 10 mm gas-tight quartz-glass cuvettes (Hellma) using UV/vis-grade solvents. The maximum ab-

sorption was kept below 0.1 at 450 nm. For obtaining the quantum yield, a three-point determination was performed. The quantum yield was obtained by taking the mean value of the three-point determination.

For determining the quantum yields, the following equation was used:

$$Q_x = Q_R \times \left(\frac{A_R}{A_X}\right) \times \left(\frac{E_X}{E_R}\right) \tag{1}$$

Q_x = emission quantum yield of the investigated compound; Q_R = emission quantum yield of the reference compound $[Ru(bpy)_3](PF_6)_2$ (Q_R = 0.095) [27]; $A_{R/X}$ = absorbance of the reference compound and the investigated compound at the excitation wavelength, respectively; $E_{R/X}$ = area under the emission curve of the reference compound and the investigated compound, respectively.

2.3. Time-Resolved Emission Studies

Fluorescence lifetimes were recorded with a DeltaPro from Horiba Scientific using a 451 nm pulsed laser source (Class 3B Laser Product, <0.5 W peak in pulsed and CW mode). The Delta Pro consists of DeltaDiode (picosecond diode controller), DeltaHub (High throughput TCSPC controller), DPS-1 (Detector Power supply), and a PPD (picosecond photon detection module). The IRF (instrument response function) was measured with LUDOX silica nanoparticles. Fits were done with the software EzTime with a mono-exponential decay.

2.4. Electrochemistry

The cyclic voltammograms were carried out in dry acetonitrile, and 0.1 M TBAPF$_6$ was used as the supporting electrolyte. The measurements were performed with an Autolab potentiostat PGSTAT204 from Metrohm using a three-electrode configuration: a glassy carbon disc with a 3 mm diameter stick (working), a Pt electrode (counter), and a non-aqueous Ag/Ag$^+$ electrode with 0.01 M AgNO$_3$ in dry acetonitrile (reference). A ferrocene/ferrocenium (Fc/Fc$^+$) couple was applied as the reference, which was added to the solution after each measurement. Thus, all reported potentials are versus the Fc/Fc$^+$ couple. All scan rates are 100 mV/s unless otherwise noted.

2.5. Mass Spectrometry

High-resolution mass spectrometry (HRMS) was recorded with a solariX (Bruker Daltonik) equipped with a 7.0 T superconducting magnet and interfaced with an Apollo II Dual ESI/MALDI.

2.6. NMR Experiments

The NMR spectra were recorded on a Bruker AVANCE 400 MHz spectrometer at ambient temperature. Chemical shift values (δ) are given in parts per million (ppm) using residual solvent protons (δH = 7.26 ppm and δC = 77.16 ppm for CDCl$_3$, δH = 1.94 ppm and δC = 118.26 ppm for CD$_3$CN, and δH = 3.31 ppm and δC = 49.05 ppm for MeOD-d$_4$) as the internal standard.

2.7. Hydrogen Determination

The amount of generated hydrogen was determined by gas chromatography (GC) on a Bruker Scion SQ with a thermal conductivity detector and argon as carrier gas (column: Mol. Sieve 5 Å 75 m $\times$ 0.53 mm I.D., oven temp. 70 °C, flow rate 25 mL min^{-1}, detector temperature 200 °C) using 100 µL of the gas phase. The GC was calibrated by the injection of different volumes of a hydrogen/argon mixture with a known hydrogen amount. The turnover number (TON) and incremental turnover frequency (TOF) were calculated by the following equations.

$$TON = \frac{n(H_2)}{n(catalyst)} \tag{2}$$

$$\text{TOF}_{\text{inkr}} = \left(\frac{n_{x+1}(\text{H}_2) - n_x(\text{H}_2)}{n(\text{catalyst}) \times (t_{x+1} - t_x)} \right) = \left(\frac{\text{TON}_{x+1} - \text{TON}_x}{t_{x+1} - t_x} \right) \tag{3}$$

t_{x+1} = time one measurement after the measurement before, n = amount of the respective compound.

2.8. Preparation of Catalytic Mixture

In a 21 mL Schlenk tube, sealed with a standard NS14 rubber septum, 0.14 μmol of the **Rup(ph)pPtX$_2$**-complex (X = Cl, I) was added by the addition of the respective volume (varying volume due to varying concentrations of the stock solution) of a dichloromethane/ **Rup(ph)pPtX$_2$** (X = Cl, I) stock solution followed by the evaporation of the solvent outside of the glovebox. In case additional salts (e.g., TBAI, TBACl) were used during catalysis, they were added at this stage. After that, introducing the tube in the glovebox and adding 7.5 mL of an acetonitrile, triethylamine, and water mixture (*v:v:v* = 6:3:1) yielded the respective 70 μM catalyst concentration. In the case of Hg addition, this was added after the complete addition of the solvent. The tube was finally sealed with an NS14 rubber septum. The irradiation of the catalytic mixtures with visible light (2 LED sticks, λ = 470 ± 20 nm, 45 ± 5 mW·cm^{-1}, suitable to excite the ^{1}MLCT transition of the complexes) was conducted outside of the glovebox for defined time intervals. The subsequent analysis of the headspace by gas chromatography determined the amount of hydrogen produced. By multiplying the TON by 0.14 μmol, the produced amount of hydrogen can be calculated. All data points were determined at least twice.

2.9. Reactor Design

The reactor was made out of steel and the design (length = 20.5 cm; width = 20 cm; height = 20 cm) is depicted in Figure S15. The Schlenk tube was fixed in the middle (distance to the walls d = 9 cm) and two LED sticks were placed in varying positions around the tube. During irradiation, the Schlenk tube was cooled by air using two air coolers per side (diameter = 9.2 cm with a power of 50.0 m^3 each) for a total of four coolers. The temperature and the pressure of the catalytic mixture during catalysis were not determined. The two LED sticks (λ = 470 ± 20 nm, per LED stick 45 ± 5 mW·cm^{-1}; for emission spectra, see Figure S24) were in close proximity to the Schlenk tube (distance d = 0 cm). We therefore assume that the photon flux of the LED sticks is identical to the irradiation power of the sample. However, since the LED sticks (total length of the LED area of 11 cm) consist of single LED points and are placed on a circuit board (length l = 30 cm) that is higher than the catalytic solution (height h = ca. 5.5 cm), the LED stick was adjusted so that the solution was completely irradiated.

3. Results and Discussion

3.1. Synthesis of the Ligand and the Complexes

The linkage of two phenanthroline spheres in the 5,5′-position can be achieved using either a direct linkage (phenphen system) [8] or by the utilization of a spacer (e.g., phenyl, triazole, alkyne) [18,28]. As described earlier, the direct C-C linkage of two phenanthroline spheres is accompanied by relatively low yields (varying between 9% and up to 35%) [8,29,30], as well as the nearly perpendicular orientation of the two 1,10-phenanthroline spheres. The introduction of a spacer seems interesting since standard cross-coupling reactions can be used to enhance the overall synthetic yield (for **p(ph)p** up to 75%) [28] as well as the flexibility of the bridging ligand itself (see below) [8].

The synthesis of the **p(ph)p** ligand was performed based on a slightly modified approach by Hossain et al. (see Scheme 1) [28]. We therefore used diborylated 1,4-bis(4,4,4,4-tetramethyl-1,2,3-dioxoborolan-2-yl)benzene and 5-bromo-1,10-phenanthroline [24], as halogen-containing phenanthroline, and performed a Suzuki cross-coupling reaction using K$_2$CO$_3$ as base and [Pd(PPh$_3$)$_2$Cl$_2$] as a catalyst (Scheme 1, step (i)) [24,28]. Instead of using column chromatography, the crude ligand was recrystallized in ethanol to remove excess

PPh$_3$ and PPh$_3$O. The ligand **p(ph)p** was obtained at a 71% yield, comparable to what has been reported in the literature (75%) [28].
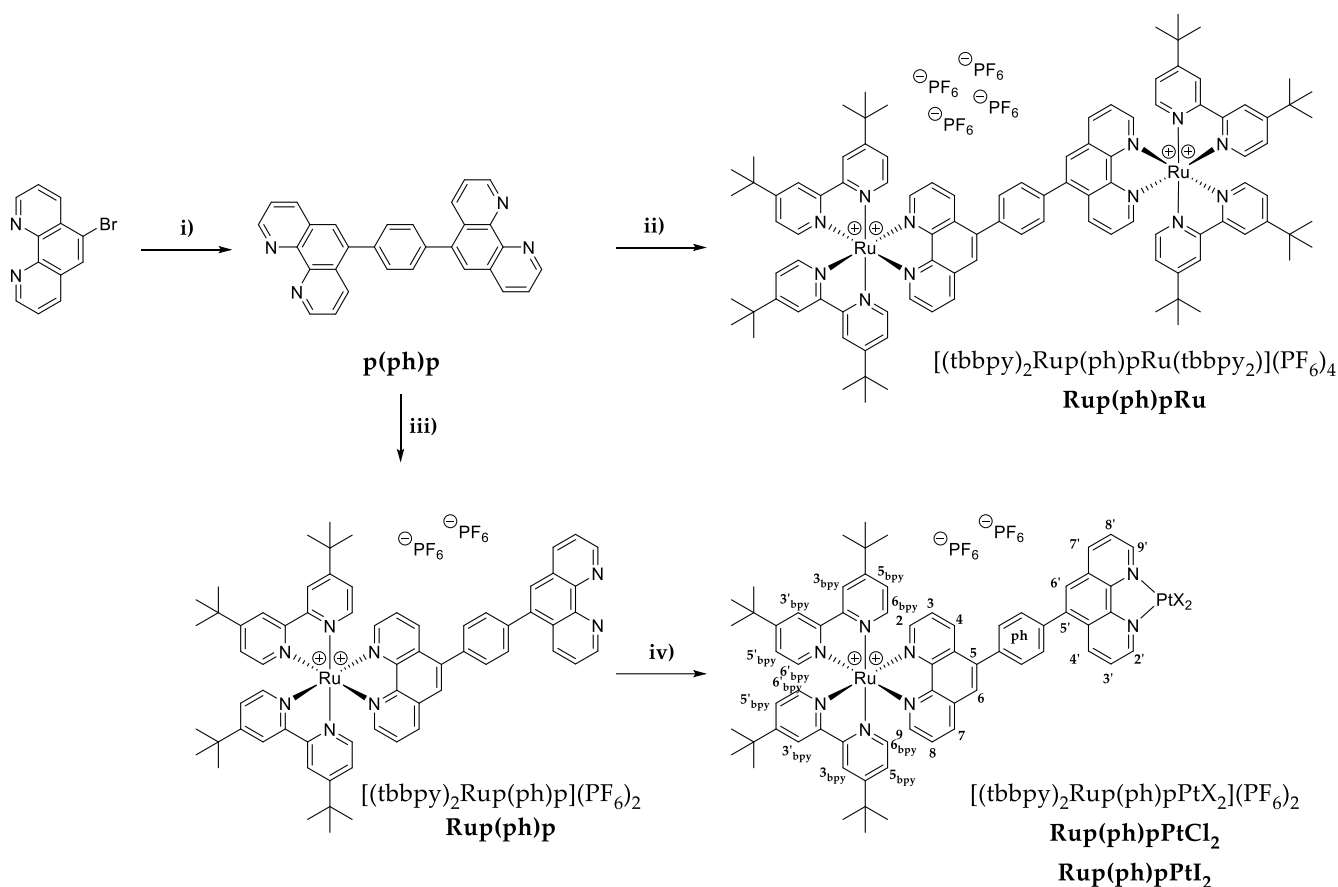
Scheme 1. Molecular structure, ^{1}H NMR assignment, and synthetic access to mono- and dinuclear ruthenium complexes of 5,5′-linked, phenyl-spaced bis-phenanthroline bridging ligands. (**i**) 1,4-bis(4,4,4-tetramethyl-1,2,3-dioxoborolan-2-yl)benzene, Pd(PPh$_3$)Cl$_2$, K$_2$CO$_3$, DMSO, 100 °C, 48–72 h; yield: 71%; (**ii**) [(tbbpy)$_2$RuCl$_2$], ethanol/ethylene glycol (*v*:*v* = 1:1), 130 °C, 3.5 h; yield: 89%; (**iii**) [(tbbpy)$_2$RuCl$_2$], ethanol/ethylene glycol (*v*:*v* = 1:1), 130 °C, 3.5 h; yield: 63.8%; (**iv**) [Pt(DMSO)$_2$X$_2$] (X = Cl, I), ethanol, reflux, 5 h; yield: 85–88%.

The coordination of the **p(ph)p** ligand to a single [(tbbpy)$_2$RuCl$_2$] precursor using standard methods [8,31], i.e., a 3:1 to 4:1 ethanol:water mixture as the solvent or microwave-assisted reactions, proved to be difficult due to the availability of the two coordination spheres of the barely soluble ligand. However, successful complexation could be achieved using a diluted **p(ph)p** ethanol/ethylene glycol solution and the slow addition of [(tbbpy)$_2$RuCl$_2$] (Scheme 1 and Scheme S1, step (iii)), following the protocol of Karnahl et al. [32], which can easily be applied to 5,5′-bis-phenanthroline-based systems [8].

Typical for ligands bearing two coordination spheres, the crude mixtures contained **p(ph)p**, **Rup(ph)p,** and homodinuclear **Rup(ph)pRu**, which could be separated by size exclusion chromatography, yielding the pure mononuclear complex at a 64% yield. Instead of collecting the dinuclear **Rup(ph)pRu** complex as a side product from the described synthesis of **Rup(ph)p**, homodinuclear **Rup(ph)pRu** was accessed directly using 2.1 equivalents of [(tbbpy)$_2$RuCl$_2$] (step (ii)) and by applying the same synthetic procedure as for **Rup(ph)p**. High yields (up to 89%) could be achieved since side-product formation is negligible. The introduction of a second metal center by the reaction of [PtCl$_2$(DMSO)$_2$] or [Pt(DMSO)$_2$I$_2$] with **Rup(ph)p** forming heterodinuclear **Rup(ph)pPtX$_2$** complexes (X = Cl, I) is feasible in high yields (up to 88%, step (iv))), irrespective of the nature of the halide ligands (X = Cl or I).

All complexes were characterized with respect to their structural, photophysical, photochemical, and electrochemical properties. The dinuclear **Rup(ph)pPtX$_2$** complexes were also investigated in their catalytic activity for light-driven hydrogen evolution.

3.2. Structural Characterization

^{1}H NMR spectroscopy of **p(ph)p** (see Supplementary Materials, Figure S1) revealed a D$_{2h}$ symmetry, as only five signals were present, which can be fully assigned using 2D NMR spectroscopy (see Figure S3). Interestingly, the solubility is much lower compared to the previously reported directly C-C-linked phenphen ligand, [8,29,33] even in chlorinated solvents such as chloroform.

Contrary to these results, the solubility of the obtained mono- and dinuclear ruthenium complexes showed no differences in comparison to the analogous phenphen-based complexes [8]. The ^{1}H NMR analysis of the aromatic region of **Rup(ph)p** revealed a higher symmetry compared to [(tbbpy)$_2$Ru(phenphen)](PF$_6$)$_2$, described earlier [8]. This indicates a much lower rotational barrier of the herein described bis-phenanthroline ligand, which can be attributed to its phenyl spacer. The higher flexibility is also visible in the other homo- and heterodinuclear complexes (Figure 2), where no evidence for diastereomers can be found, contrary to the phenphen-based Ru complexes, where true atropisomers were observed [8].
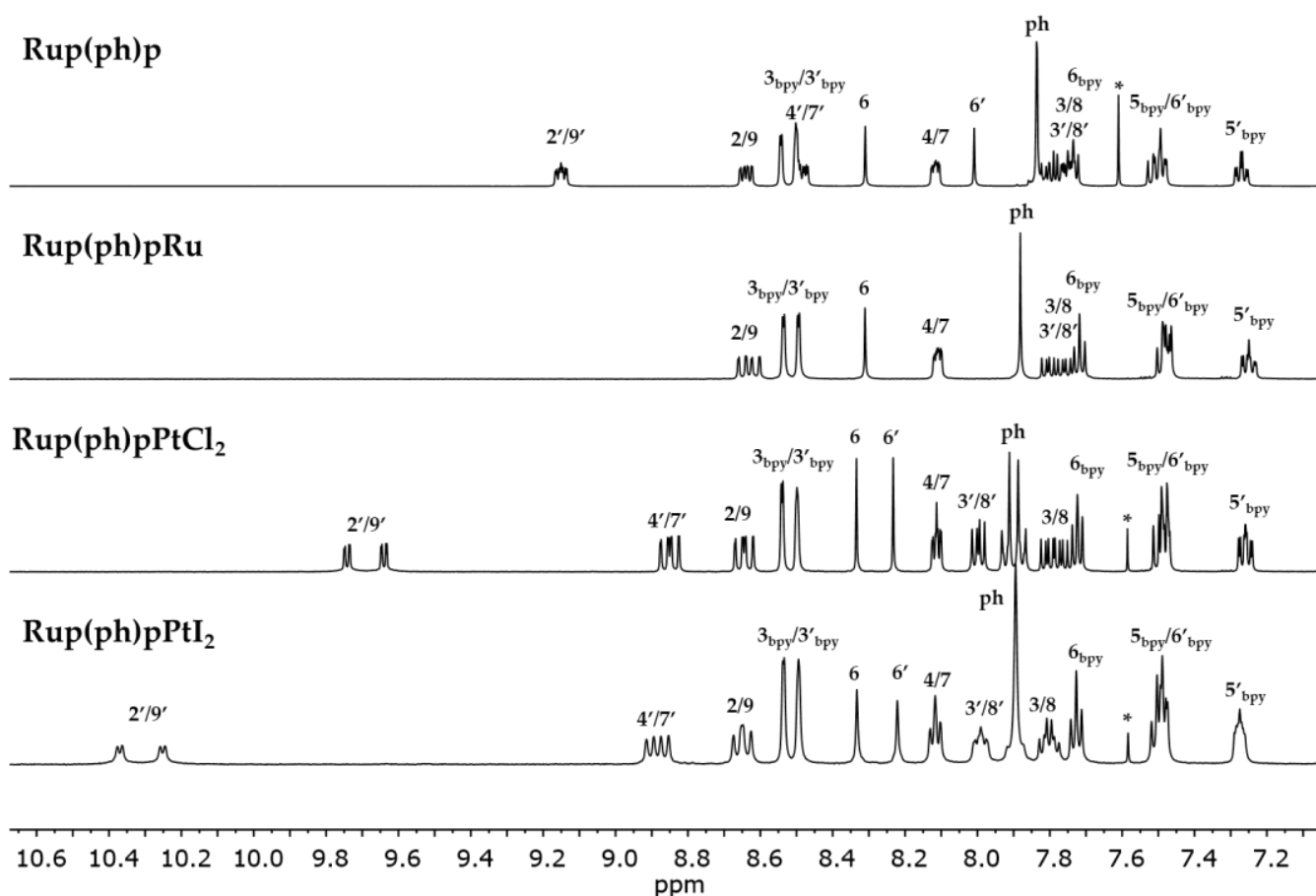
Figure 2. ^{1}H NMR spectra (400 MHz) of the aromatic region of **Rup(ph)p**, **Rup(ph)pRu**, **Rup(ph)pPtCl$_2$**, and **Rup(ph)pPtI$_2$** in deuterated acetonitrile at room temperature. The signal marked with an asterisk can be assigned to leftover chloroform (7.58 ppm). For the assignment of the individual peaks, see Scheme 1 as well as Figure S3.

A clear splitting of the phenanthroline-based 6/6′-proton is observed, which results from the different chemical environments at the ruthenium-bound and the non-/second

metal-bound coordination spheres. The coordination of a second metal center shifts the unbound $6'$-proton from 8.01 ppm to 8.31 ppm in the case of **Rup(ph)pRu**, and to 8.23 ppm in the case of **Rup(ph)pPtCl₂** and **Rup(ph)pPtI₂**, respectively.

Additionally, the effect of coordinating a second metal center can be clearly observed by the shifts of the $2'/9'$-protons of the second coordination sphere, which shifts to lower ppm values for the homoleptic, dinuclear **Rup(ph)pRu** and to higher ppm values with the introduction of a platinum center. Interestingly, the introduction of the iodide anion shows a significant influence on the shifts of the $2'/9'$ protons, causing a deshielding of the protons (approx. 10.3 ppm compared to 9.7 ppm). However, via ¹⁹⁵Pt NMR spectroscopy (Figure S6), it was observed that an exchange from chloride (−2331.90 ppm) to iodide (−2285.46 ppm) causes the shielding of the Pt center, which is reflected in a strong shift of approx. 45 ppm.

3.3. Photophysical Characterization

The ground-state absorption and excited-state emission of the different Ru complexes (³MLCT-state) are shown in Figure 3. All four complexes show two absorption bands centered at 275 nm and at around 450 nm, typical for Ru polypyridine complexes and comparable to the previously reported phenphen-based systems [8]. According to the literature, the band at 450 nm can be assigned to the MLCT absorption band, while the band at 275 nm is attributed to ligand-based π-π*-interactions [8,22,34]. The position of the absorption maximum and the extinction coefficient of the mononuclear **Rup(ph)p** (455 nm, 18.33×10^3 M⁻¹ cm⁻¹) is comparable to the Pt-containing complex **Rup(ph)pPtCl₂** (455 nm, 17.99×10^3 M⁻¹ cm⁻¹) indicating no notable influences on the main photophysical properties of the introduced Pt center. Interestingly, **Rup(ph)pPtI₂** (452 nm, 19.00×10^3 M⁻¹ cm⁻¹) provides a second absorption maximum at approx. 425 nm. The comparison of the ¹MLCT absorption maximum of [Pt(bpy)I₂] at 385 nm (approx. 5.0×10^3 M⁻¹ cm⁻¹; ¹MLCT (Pt → phen)) with the maximum in **Rup(ph)pPtI₂** at approx. 425 nm indicates a superimposition of the absorption spectra of **Rup(ph)p** and [Pt(bpy)I₂] [35]. This hypothesis is also reflected in the shoulder of **Rup(ph)pPtCl₂** at approx. 390 nm, which is nearly identical to the ¹MLCT absorption maximum of pure [Pt(phen)Cl₂] [36]. As expected, homodinuclear **Rup(ph)pRu,** containing two Ru centers, provided a doubled extinction coefficient but no shift in the absorption maximum (455 nm, $37.59 \cdot \times 10^3$ M⁻¹ cm⁻¹) compared to the mononuclear complexes. The ³MLCT emission maxima of all three dinuclear complexes (614–617 nm) are comparable and do not provide any significant shifts in air-saturated acetonitrile (see Table 1). The dinuclear homoleptic **Rup(ph)pRu** shows the same emission intensity per ruthenium core and a doubled emission intensity for the same concentration, since two ruthenium centers are absorbing and emitting photons. We can therefore conclude that the bridging ligand provides a very limited electronic interaction between the two coordination spheres.

Interestingly, the introduction of a Pt center does not lead to a decreased quantum yield of ³MLCT emission in acetonitrile ($\phi_{\text{Rup(ph)p}}$ = 0.01 vs. $\phi_{\text{Rup(ph)pPt}}$ = 0.01) under air-saturated conditions. These results are in accordance with the previously published [(tbbpy)₂Ru(phenphen)](PF₆)₂-system, as ³O₂ is the predominant quencher resulting in the decreased quantum yield in an air-saturated (ϕ = 0.01) compared to an argon-saturated (ϕ = 0.11–0.20) environment [8]. This is also reflected in the similar emission lifetimes of the four Ru complexes (τ = 107–111 ns, see Table 1) under air-saturated conditions, which are significantly lower compared to the argon-saturated measurements (τ = 1512–2046 ns).

As described above, no influence of the second metal center can be detected in the air-saturated solutions, and enhanced emission quantum yields under argon-saturated conditions are observed. (Table 1). The emission quantum yields of **Rup(ph)p** (ϕ = 0.19), **Rup(ph)pRu** (ϕ = 0.20), and **Rup(ph)pPtCl₂** (ϕ = 0.19) provide no evidence for an interaction of the second coordination sphere with the ³MLCT state since there is no detectable quenching by the PtCl₂ center.
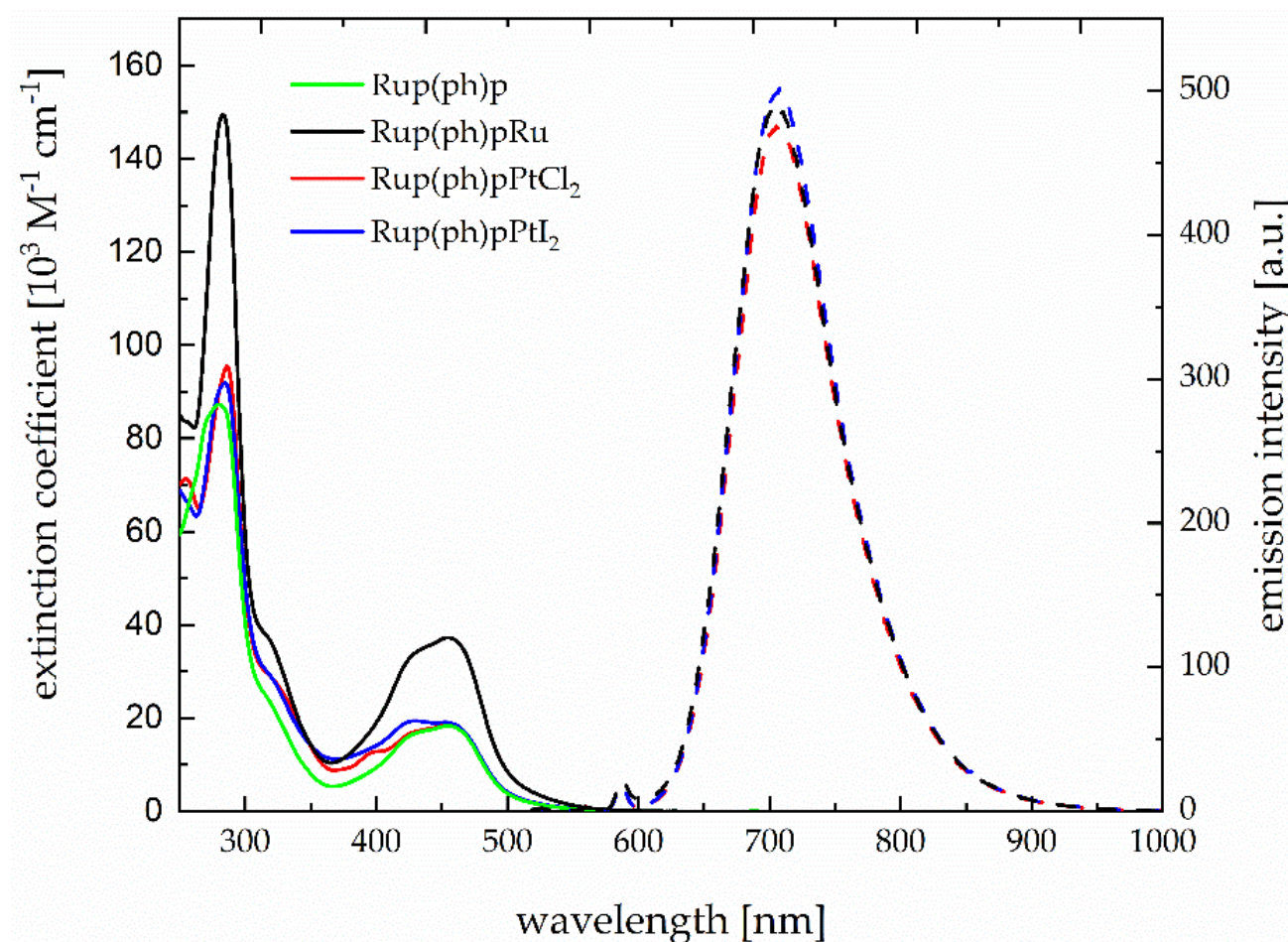
Figure 3. Absorption and emission (λ_{exc} = 450 nm) spectra of **Rup(ph)p**-type complexes in air-saturated acetonitrile. The emission intensity of dinuclear **Rup(ph)pRu** is measured at a concentration of $2.5 \cdot \times 10^{-6}$ M, while for all other Ru compounds the concentration was $5 \cdot \times 10^{-6}$ M.

Table 1. Spectroscopic data of the ruthenium complexes collected in acetonitrile under [b] air-saturated and [c] argon-saturated conditions.

Complex	$\lambda_{max,abs}$ [nm] (ϵ, 10^3 M^{-1} cm^{-1}) [a]	$\lambda_{max,emi}$ [nm][a,b]	ϕ_{em}[a,b]	$\phi_{em}^{-O_2}$[b,c]	τ^{O_2}[ns][a,d]	τ^{-O_2}[ns][c,d]
Rup(ph)p	455 (18.33)	617	0.01	0.19	110	1848
Rup(ph)pRu	455 (37.59)	615	0.01	0.20	111	2046
Rup(ph)pPtCl$_2$	455 (17.99)	614	0.01	0.19	109	1647
Rup(ph)pPtI$_2$	452 (19.00)	614	0.01	0.11	107	1512
[Ru(tbbpy)$_3$]$^{2+}$ [37–39]	458 (17.34)	613	0.01	0.05	107	730
[(tbbpy)$_2$Ru(phen)]$^{2+}$ [40]	454 (16.00)	610	–	–	211	1423
[(tbbpy)$_2$Ru(phenphen)]$^{2+}$ [8]	454 (18.68)	618	0.01	0.20	127	2000

ϕ_{em} = quantum yield, τ^{O_2}/τ^{-O_2} = emission lifetime, phen = 1,10-phenanthroline. [a] air-saturated. [b] relative measurements compared to [Ru(tbbpy)$_3$](PF$_6$)$_2$ excited at 450 nm [27]. [c] argon-saturated. [d] λ_{exc} = 451 nm.

However, with **Rup(ph)pPtI$_2$**, a notable quenching of the emitting ^{3}MLCT state can be observed (ϕ = 0.11), with the emission intensity reduced by almost 50% compared to the other systems. We hypothesize that the higher electron density at the Pt center (reflected in the lower shift in the ^{195}Pt NMR of the iodide derivative) leads to a stronger interaction between the initially populated Ru-centered ^{3}MLCT state and the Pt center. This is in line with the emission lifetime in argon-saturated acetonitrile given that **Rup(ph)pPtI$_2$** provided

the lowest lifetime (τ = 1512 ns) in the series of these four **Rup(ph)p**-based complexes (see Table 1 and Figures S11 and S12).

3.4. Photochemical Characterization

For all complexes, calculations on their photostabilities were performed by the evaluation of the loss of their ^{1}MLCT absorption maxima in air-saturated acetonitrile solutions (Figures S16–S19 and Table S1) when illuminated with blue light (λ = 470 $\pm$ 20 nm; 45 $\pm$ 5 mW·cm^{-1}). Interestingly, **Rup(ph)p** (63% loss in 24 h) provided the lowest photostability compared to **Rup(ph)pRu** (44% loss in 24 h), **Rup(ph)pPtCl$_2$** (54% loss in 24 h), and **Rup(ph)pPtI$_2$** (42% loss in 24 h). Compared to the previously reported [(tbbpy)$_2$Ru (phenphen)](PF$_6$)$_2$ system [8], the photostability of all the new dinuclear complexes is notably lower compared to the phenphen-based analogs. For [(tbbpy)$_2$Ru(phenphen)Ru (tbbpy)$_2$](PF$_6$)$_4$ and [(tbbpy)$_2$Ru(phenphen)PtCl$_2$](PF$_6$)$_2$, a rather high photostability was observed (only a 17% loss in 24 h for the homodinuclear and 19% loss in 24 h for the heterodinuclear system, respectively).

3.5. Electrochemical Characterization

Fully reversible electrochemistry, comparable to standard [Ru(bpy)$_3$]$^{2+}$-type complexes, was observed for **Rup(ph)p** and **Rup(ph)pRu**, while both heterodinuclear complexes **Rup(ph)pPtX$_2$** revealed multiple irreversible (irr) redox processes of the ligands in an argon-saturated acetonitrile solution containing 0.1 M nBu$_4$NPF$_6$ as the supporting electrolyte (Table 2 and Figure S21). This is in accordance with the related tpphz-based dinuclear system [12]. In general, all complexes provided at least three ligand-based reduction waves at approx. -1.73 V, -2.00 V, and -2.30 V as well as a metal-centered oxidation wave at approx. 0.79 V (Ru^{2+}/Ru^{3+}) vs. Fc^0/Fc$^+$ (Table 2), which is comparable to [Ru(bpy)$_2$(phen)]$^{2+}$ and [(tbbpy)$_2$Ru(phenphen)]$^{2+}$ [8,40]. The fact that the redox potential of the Ru^{2+}/Ru^{3+} step is insensitive to the presence of a second metal center supports the assumption that the bridging ligand does not provide strong interaction between the two metal centers [41].

Table 2. Redox potentials $E_{1/2}$ (V) of **Rup(ph)p**-type complexes in argon-saturated dry acetonitrile with 0.1 M nBu$_4$NPF$_6$ as a supporting electrolyte, referenced against Fc^0/Fc$^+$. All CVs are depicted in Figure S21 in the supporting information.

Complex	L$_3$ [V]	L$_2$ [V]	L$_1$ [V]	L$_0$ [V]	Ru^{2+}/Ru^{3+} [V]
Rup(ph)p	-2.24	-2.00	-1.73	–	0.79
Rup(ph)pRu	-2.28	-1.99	-1.70	–	0.79
Rup(ph)pPtCl$_2$	-2.30	-2.03	-1.73 (irr)	-1.57	0.79
Rup(ph)pPtI$_2$	-2.31 (irr)	-1.97	-1.74 (irr)	-1.60 (irr)	0.84
[Ru(tbbpy)$_3$]$^{2+}$ [42]	-2.28	-2.01	-1.80	–	0.73
[Ru(bpy)$_2$(phen)]$^{2+}$ [40]	-2.25	-1.98	-1.77	–	0.74
[Ru(phenphen)]$^{2+}$ [8]	-2.25	-1.98	-1.72	–	0.80

L$_0$, L$_1$, L$_2$, and L$_3$: redox events correlated to the ligand spheres at the Ru center.

However, **Rup(ph)pPtI$_2$** provided three irreversible redox events (L$_3$, L$_1$, and L$_0$), and **Rup(ph)pPtCl$_2$** provided one (L$_1$) out of four. We attribute this higher electrochemical instability of the PtI$_2$ derivative to its higher electron density at the Pt center, making the reduced states of the ligands even more reactive for reduction-induced side reactions [12].

For the two **Rup(ph)pPtX$_2$** complexes, the reduction event L$_1$ at approx. -1.74 V is reflected as an irreversible redox wave (shoulder), while for **Rup(ph)p** and **Rup(ph)pRu**, a reversible redox wave can be observed. In the case of **Rup(ph)pPtCl$_2$**, we observed a new reversible redox event L$_0$ at -1.57 V, while for **Rup(ph)pPtI$_2$**, the redox event at -1.60 V was irreversible, which most likely indicates the reduction of a ligand–Pt mixed orbital. Interestingly, this reduction was not observed for the [(tbbpy)$_2$Ru(phenphen)PtCl$_2$](PF$_6$)$_2$ complex [8]. However, a complete disruption of the conjugation between the ruthenium

and the platinum moiety would be represented by two reduction waves at approx. −1.71 V and −1.13 V for [(phen)PtCl$_2$] [43–45]. So far, we were not able to clearly distinguish whether complete disruption occurs, as the observed reduction wave at −1.13 V was neither visible for **Rup(ph)pPtCl$_2$** nor **Rup(ph)pPtI$_2$**.

3.6. Light-Induced Evolution of Molecular Hydrogen

The ability for photocatalytic hydrogen evolution by **Rup(ph)pPtCl$_2$** and **Rup(ph)pPtI$_2$** was tested using 7.5 mL of a 70 μM catalytic solution (*v:v:v* = 6:3:1; acetonitrile:triethylamine:water) in a Schlenk tube, illuminated with two LED sticks (each of them characterized by λ_{emi} = 470 ± 20 nm and P = 45 ± 5 mW·cm^{-2}) in a custom-made, air-cooled photoreactor (see Figure S15). During the course of several hours, samples were taken from the headspace and the produced hydrogen amount was determined by repeated GC-TCD measurements (see Figure 4).
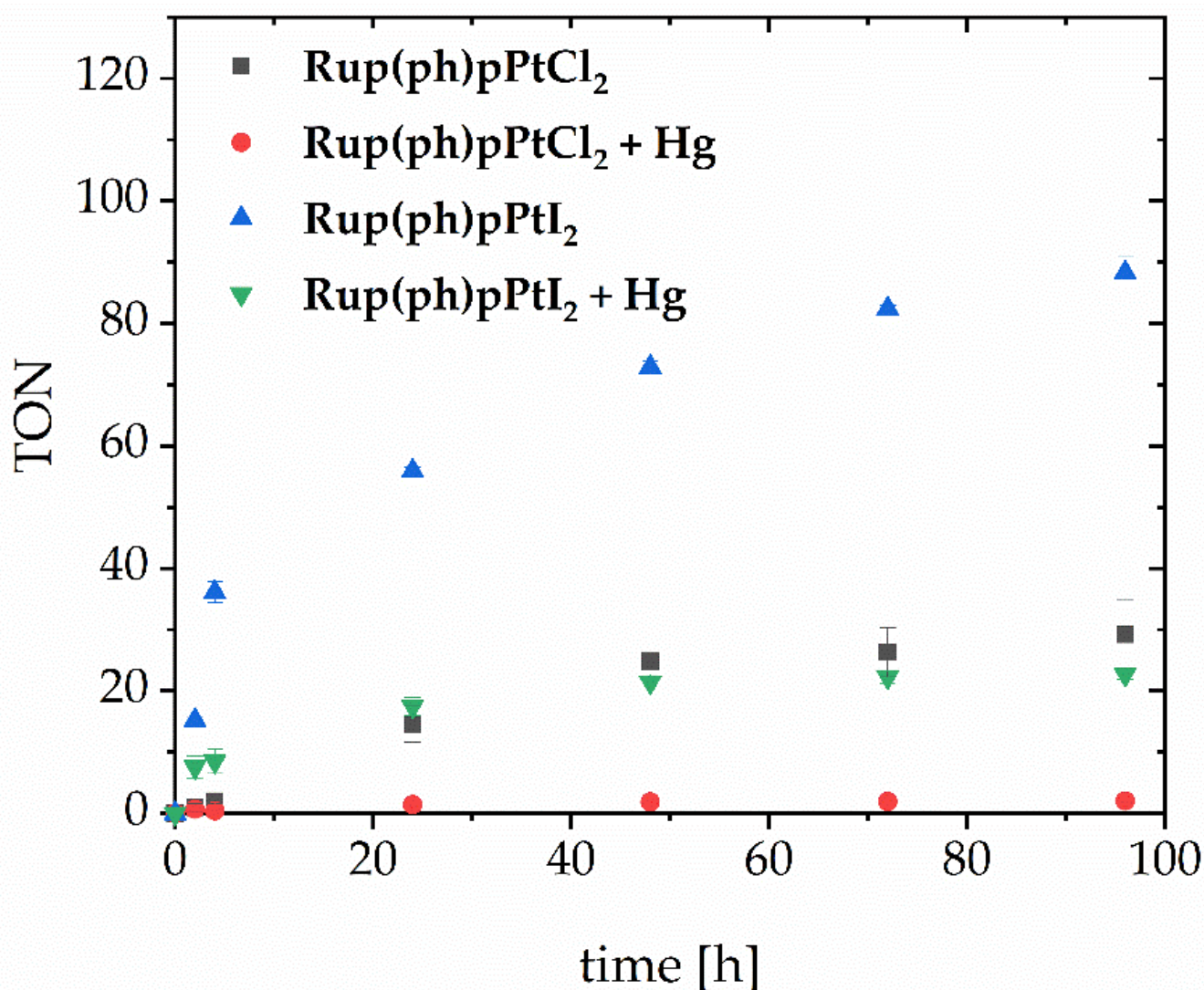

Figure 4. Catalytic activity of **Rup(ph)pPtCl$_2$** and **Rup(ph)pPtI$_2$** with and without the addition of elemental mercury in an argon-saturated 6:3:1 (*v:v:v* = acetonitrile:triethylamine:water) mixture irradiated with two LED sticks (each of them characterized by λ_{emi} = 470 ± 20 nm and P = 45 ± 5 mW·cm^{-2}) under air cooling. Error bars represent the standard deviation for two individual measurements. Error bars represent standard deviations based on n = 2 independent measurements.

Interestingly, an increased overall hydrogen evolution of **Rup(ph)pPtI$_2$** (TON$_{96h}$ = 88.3 ± 2.5) compared to **Rup(ph)pPtCl$_2$** (TON$_{96h}$ = 29.2 ± 5.7) was observed. In addition, the maximum TOF of 10.5 ± 0.6 h^{-1} is already obtained after 4 h for the PtI$_2$ derivative, while for the PtCl$_2$ derivative, the maximum TOF of 0.6 ± 0.1 h^{-1} is only obtained after 24 h.

This points not only towards a different mechanism for the light-driven hydrogen evolution by the two dinuclear photocatalysts but it is also in line with previous results on the [(tbbpy)$_2$Ru(tpphz)PtX$_2$](PF$_6$)$_2$ (X = Cl, I) system, where the iodide ligand enhanced electron density at the catalytic center and therefore increased overall catalytic activity by presumably boosting the efficiency of forming the important Pt(III)-H intermediate, as proposed by Sakai [12,46–48]. Nevertheless, the **p(ph)p**-based system is less active than the related tpphz-bridged system, where under identical conditions, a TON of 188 after 70 h has been observed for the PtI$_2$ derivative [12]. In the case of the PtCl$_2$ derivative, the introduction of the phenyl-spacer between the two phenanthroline spheres did not enhance the catalytic activity; instead, a lower output by approx. 15 TON within 96 h, compared to the previously published [(tbbpy)$_2$Ru(phenphen)PtCl$_2$](PF$_6$)$_2$ system (TON$_{96h}$ = 44), was observed [8].

To gain insight into whether molecular or colloid-driven catalysis occurs, the mercury test was performed. [7,8,49–51] It clearly demonstrated colloid-driven catalysis for **Rup(ph)pPtCl$_2$**, as the catalytic activity was significantly decreased (TON$_{96h}$ = 29.2 compared to TON$_{96h,Hg}$ = 2.1). Surprisingly, in the presence of Hg, **Rup(ph)pPtI$_2$** was by a factor of 10 more active (TON$_{96h,Hg}$ = 23.7) compared to **Rup(ph)pPtCl$_2$** (TON$_{96h,Hg}$ = 2.1). However, also for **Rup(ph)pPtI$_2$**, decreased catalytic activity was observed when Hg was added to the solution (TON$_{96h}$ = 88.3 vs. TON$_{96h,Hg}$ = 29.2). To exclude the chemical instability of **Rup(ph)pPtCl$_2$** and **Rup(ph)pPtI$_2$** against mercury prior to irradiation as a possible reason for the reduced photocatalytic activity, both complexes were stirred in air-saturated acetonitrile and five drops of elemental mercury were added, representing a high load of Hg. After 24 h, the ^{1}H NMR spectra after Hg stirring with the initial spectra prior to Hg addition were compared. No differences were observed in the case of **Rup(ph)pPtCl$_2$** (Figure S4), while for **Rup(ph)pPtI$_2$** (Figure S5) the quantitative loss of the Pt center was monitored. Furthermore, high-resolution ESI-MS was performed in the case of the PtI$_2$-derivative, clearly showing only **Rup(ph)p** as the final Ru-derived decomposition product (Figure S10) from the treatment of **Rup(ph)pPtI$_2$** with Hg. This is in accordance with the previously published results for [(tbbpy)$_2$Ru(tpphz)PtI$_2$](PF$_6$)$_2$, which has also not been stable against mercury prior to irradiation [12] while [(tbbpy)$_2$Ru(tpphz)PtCl$_2$](PF$_6$)$_2$ did not show any signs of degradation during Hg treatment [7]. The combination of these datasets indicates that **Rup(ph)pPtCl$_2$** evolves hydrogen exclusively via a colloid-driven mechanism, while **Rup(ph)pPtI$_2$** initially produces hydrogen by a molecular pathway, then gradually turns into a colloid-driven process. The phase of molecular operation by the PtI$_2$ derivative is also manifested in a rapid increase in hydrogen gas during the first hours of irradiation in the absence of Hg, in which a very similar TOF for **Rup(ph)pPtI$_2$** (TOF = 5–10 h^{-1}) as for the fully molecularly operating [(tbbpy)$_2$Ru(tpphz)PtI$_2$](PF$_6$)$_2$ (TOF = 5–8 h^{-1}) is observed. The subsequent decrease in catalytic activity for **Rup(ph)pPtI$_2$** is attributed to ligand exchanges at the Pt center, which likely induce the colloid formation, as described by Sakai et al. (see below for spectral evidence) [52].

To elucidate the influence of basic conditions (e.g., the addition of TEA or NaOH) on the stability of **Rup(ph)pPtI$_2$**, ^{1}H NMR investigations of the respective 2:1 methanol:acetonitrile mixtures were performed in the absence of light. The addition of TEA to the solution of the dinuclear complex initially caused no shifts of the 2′/9′-protons. However, after 1 h, a new signal appeared at approx. 9.7 ppm, indicating an intermediate that is subsequently converted to a final decomposition product within four days, as indicated by the complete loss of the 2′/9′-proton peak that is characteristic of intact dinuclear **Rup(ph)pPtI$_2$** (see Figure S25). The same decomposition product was quickly obtained within two hours when NaOH was added to the 2:1 methanol:acetonitrile solution of **Rup(ph)pPtI$_2$** (see

Figure S25), as well as within 9 h by the exchange of the methanol:acetonitrile solution against the catalytic solution (see Figure S29). It is thus concluded that under basic conditions, ligand exchanges at the Pt center of **Rup(ph)pPtI$_2$** lead to the formation of Pt colloids, as proposed by Sakai and co-workers [52]. An additional reason for the reduced TON$_{96h}$ for the I-based system in the presence of Hg is likely given by the light-independent loss of the Pt center occurring in parallel with hydrogen evolution (see Figure S5). Similar to the results of treating the dinuclear complexes with Hg in the absence of light and in contrast to **Rup(ph)pPtI$_2$**, the Cl-derivative **Rup(ph)pPtCl$_2$** proved to be stable in the presence of TEA and for at least two hours in the presence of NaOH. After 9h, some decomposition products were observed for **Rup(ph)pPtCl$_2$** (see Figures S26 and S27). However, due to the higher stability of **Rup(ph)pPtCl$_2$**, it is concluded that colloid formation is a light-activated process.

To further analyze the mechanism of the photocatalytic hydrogen evolution, hydrogen amounts were determined in shorter time intervals (Figure S22), with and without the addition of TBAI and mercury, respectively. Within the first 50 min, an increase in catalytic activity ("activation") with the addition of mercury, as well as 200 eq. of TBAI, was clearly observed for **Rup(ph)pPtCl$_2$** (TON$_{30min,Hg,TBAI}$ = 3.47 vs. TON$_{30min,TBAI}$ = 1.53). Due to the absence of an induction period in the presence of Hg compared to the mixture when only **Rup(ph)pPtCl$_2$** and TBAI were present in the solution (see Figure S22), a Hg-accelerated Cl-I exchange is postulated. This has been reported in the case of the related phenphen-based system, and Cl-I exchange was also observed via ^{1}H NMR spectroscopy for the herein reported photocatalysts, where a clear shift of the $2'/9'$-protons is shown (see Figure S26). The Hg-accelerated halide exchange process is likely followed by a subsequent decomposition of the newly formed iodide complex, comparable to the phenphen-system and in accordance with the instability of **Rup(ph)pPtI$_2$** in the presence of Hg (Figure S5) [8].

However, for **Rup(ph)pPtI$_2$**, activation was also observed even without the further addition of TBAI (TON$_{20min,Hg}$ = 2.91 vs. TON$_{20min}$ = 1.71). Interestingly, the addition of Hg changes the catalytic mechanism, as no induction period was observed for **Rup(ph)pPtI$_2$**, contrary to **Rup(ph)pPtI$_2$** without Hg (see Figure S22). These results are in line with the previously reported phenphen system [8]. For **Rup(ph)pPtCl$_2$**, however, no increase in catalytic activity in the presence of only Hg was observed. In contrast, previous work on the [(tbbpy)$_2$Ru(tpphz)PtCl$_2$](PF$_6$)$_2$ system indicated an activity increase by adding only Hg [7].

Circumventing the Hg-induced instability of **Rup(ph)pPtI$_2$** and adding only 200 eq. of TBAI and no Hg to catalytic solutions of **Rup(ph)pPtCl$_2$** enhanced the catalytic activity (TON$_{5h,TBAI}$ = 17.8 compared to TON$_{5h}$ = 2.6), which is comparable to the activity-boosting effect observed for [(tbbpy)$_2$Ru(phenphen)PtCl$_2$](PF$_6$)$_2$ [8]. Based on the photo-independent halide exchange described above, we can explain the higher activity of **Rup(ph)pPtCl$_2$** in the presence of TBAI by the fast, in situ conversion of **Rup(ph)pPtCl$_2$** to **Rup(ph)pPtI$_2$**. It is important to note that the high lability of the chloride ligands at the Pt center was not observed for [(tbbpy)$_2$Ru(tpphz)PtCl$_2$]$^{2+}$ (see also Figure S27), which explains the non-existent activity-boosting effect of TBAI's addition to this catalyst. This is likely associated with a strong influence of the BL architecture on the strength of the Pt-X bonds [12,53].

Furthermore, the addition of 200 eq. of TBAI and no Hg to **Rup(ph)pPtI$_2$** for this system resulted in an increase in catalytic activity (TON$_{5h,TBAI}$ = 36.2 compared to TON$_{5h}$ = 24.7), although the activity-boosting effect was not as pronounced as for the PtCl$_2$-based photocatalyst. To analyze whether the activation of **Rup(ph)pPtI$_2$** is caused by the TBA cation, as previously reported [54], we also measured the hydrogen evolution of **Rup(ph)pPtI$_2$** with the addition of 200 eq. of TBACl. Neither observed a notable influence of the TBA cation, nor of the chloride (TON$_{5h}$ = 24.7 compared to TON$_{5h,TBACl}$ = 21.3). This not only indicates that TBA cations do not represent the cause of the increased catalytic activity of the **Rup(ph)pPtI$_2$**/TBAI system, but also that the I ligands are tightly bound to the Pt center and are not efficiently substituted by Cl. A similar result has previously been re-

ported for the tpphz-based system, where the addition of TBACl also did not lead to a drop in catalytic activity, which would have resulted from an I-Cl exchange [12]. Given that very similar photocatalytic activity has been observed for **Rup(ph)pPtI₂**, **Rup(ph)pPtI₂** in the presence of 200 eq. TBACl, as well as **Rup(ph)pPtCl₂** in the presence of 200 eq. TBAI (see Figure S23), it is therefore concluded that **Rup(ph)pPtI₂** is the thermodynamically favored halide-bound species and that **Rup(ph)pPtI₂** is efficiently formed from **Rup(ph)pPtCl₂** and TBAI. The increase in the catalytic activity of **Rup(ph)pPtI₂** with excess TBAI may therefore be attributed to a stabilization of the coordination environment at the Pt center under catalytic conditions, leading to less efficient iodide loss by the solvent or base and thus the stabilization of the molecular active species. This further supports the hypothesis that the main decomposition pathway occurs via a halide–hydroxo ligand exchange at the Pt center and subsequent particle formation, as described by Sakai et al. [52].

To further boost the catalytic activity of **Rup(ph)pPtI₂**, we also added NaSCN, as described by Sakai [47]. However, we did not observe any activation. Instead, a complete loss of photocatalytic activity ($TON_{5h} = 0$, see Figure S23) was observed. By analyzing a **Rup(ph)pPtI₂**/NaSCN mixture in 2:1 methanol:acetonitrile using ^{1}H NMR spectroscopy, we clearly observed immediate iodide–thiocyanide ligand exchange at the Pt center (see Figure S25). It is therefore concluded that the in situ-formed $Pt(SCN)_2$ complex is inactive towards hydrogen evolution and the halide ligands at the Pt center are necessary for allowing light-driven hydrogen evolution.

4. Conclusions

Herein, we reported the straightforward synthetic access to **Rup(ph)p**-type homo- and heterodinuclear complexes. All Ru complexes were fully characterized with respect to their structural, photophysical, photochemical, and electrochemical properties, as well as the catalytic activity for the light-driven hydrogen evolution of the Pt complexes. Interestingly, the **Rup(ph)pPtX₂** (X = Cl, I) systems revealed some notable differences, e.g., in ^{195}Pt NMR and emission spectroscopy.

In addition, HER studies clearly demonstrated that **Rup(ph)pPtI₂** is notably more active compared to its chloride analog **Rup(ph)pPtCl₂**, similar to what has been observed for the related tpphz-bridged dinuclear systems [12]. It was not only demonstrated that the nature of the halide ligand at the Pt center influenced the mechanism by which H_2 was photocatalytically produced (**Rup(ph)pPtCl₂** forms H_2 exclusively via a colloidal mechanism and **Rup(ph)pPtI₂** initially via a molecular pathway), but it was also shown that the addition of TBAI to **Rup(ph)pPtCl₂** caused a notable increase in catalytic activity due to efficient chloride–iodide ligand exchange at the Pt center. Such an efficient Cl-I exchange process has also been observed for the $[(tbbpy)_2Ru(phenphen)PtCl_2]^{2+}$-system reported previously [8]. As for the molecularly operating photocatalyst $[(tbbpy)_2Ru(tpphz)PtCl_2]^{2+}$, this rapid Cl-I exchange does not occur [12], so it can be concluded that the chemical stability of these dinuclear photocatalysts under photocatalytic conditions is also strongly influenced by the nature of the bridging ligand, which modulates the rate of (detrimental) ligand exchanges at the Pt site. Therefore, the ability to undergo in situ activity-boosting Cl-I-exchange is correlated with the lower stability of the dinuclear photocatalyst during H_2 evolution.

By a series of different ^{1}H NMR experiments, it was further demonstrated that under basic conditions, **Rup(ph)pPtI₂** is not stable. As **Rup(ph)pPtCl₂** did not undergo any structural changes under identical conditions, the colloid formation of the Cl-based system is thus a light-activated process. Consequently, the photocatalytic as well as the ligand exchange behavior of **Rup(ph)pPtI₂** is in accordance with the hypothesis of Sakai et al. [52], stating that the formation of a hydroxo species might induce instability and opens the possibility of subsequent particle formation.

Finally, as no further stabilization of the Pt center is possible without synthetically redesigning the bridging ligand, such as equipping it with stabilizing moieties [55], the introduction of a significantly more stable catalytic center (e.g., Rh) [18] should be pursued

to allow for determining clear structure–activity relationships in new photocatalytically active dyads.

Supplementary Materials: The following supporting information can be downloaded at: https://www.mdpi.com/article/10.3390/photochem2040053/s1, Figure S1: ^{1}H NMR spectra of all compounds; Figure S2: ^{13}C NMR spectra of all compounds; Figure S3: Two-dimensional NMR spectra; Figure S4: ^{1}H NMR spectrum of **Rup(ph)pPtCl$_2$** before and after the addition of Hg; Figure S5: ^{1}H NMR spectrum of **Rup(ph)pPtI$_2$** before and after the addition of Hg; Figure S6: ^{195}Pt NMR spectra of both Pt compounds; Figure S7: ESI-MS of **p(ph)p**; Figure S8: MALDI-MS of **Rup(ph)p**; Figure S9: ESI-MS of **Rup(ph)pPtI$_2$**; Figure S10: ESI-MS of **Rup(ph)pPtCl$_2$**; Figure S11: Emission lifetimes in aerated acetonitrile; Figure S12: Emission lifetimes in argon-saturated acetonitrile; Figure S13: Logarithmic depiction of single photon counts for inert emission lifetime determination. Figure S14: Logarithmic depiction of single photon counts for aerated emission lifetime determination. Figure S15: Catalysis setup; Figure S16: Photostability of **Rup(ph)p**; Figure S17: Photostability of **Rup(ph)pRu**; Figure S18: Photostability of **Rup(ph)pPtCl$_2$**; Figure S19: Photostability of **Rup(ph)pPtI$_2$**; Figure S20: UV-Vis absorption of [(tbbpy)$_2$Ru(MeCN)$_2$]$^{2+}$; Figure S21: Cyclic voltammogram of Ru complexes; Figure S22: Catalytic activity of Pt complexes; Figure S23: Catalytic activity of Pt complexes with varying anions; Figure S24: Emission profile LED sticks; Figure S25: ^{1}H NMR spectra of **Rup(ph)pPtI$_2$** with various bases and NaSCN; Figure S26: ^{1}H NMR spectra of **Rup(ph)pPtCl$_2$** with various bases and TBAI; Figure S27: ^{1}H NMR spectra of **Ru(tpphz)PtCl$_2$** with various bases and TBAI; Figure S28: ^{1}H NMR spectra of **Rup(ph)pPtCl$_2$** with NaOH and TBAI after 9 h; Figure S29: ^{1}H NMR spectra of **Rup(ph)pPtCl$_2$** with TEA and of **Rup(ph)pPtI$_2$** under catalytic conditions after 9 h; Scheme S1: Full synthesis scheme for investigated samples. Table S1: Photostability data.

Author Contributions: Conceptualization, M.L., A.K.M. and S.R.; methodology, M.L., A.K.M., and S.R.; validation M.L.; formal analysis, M.L., S.V., M.K. and M.M.; investigation, M.L., S.V., M.K. and M.M.; resources, S.R.; data curation, M.L., S.V., M.K. and M.M.; writing—original draft preparation, M.L.; writing—review and editing, M.L., M.K., A.K.M. and S.R..; visualization, M.L.; supervision, A.K.M. and S.R.; project administration, M.L., A.K.M. and S.R.; funding acquisition, S.R. All authors have read and agreed to the published version of the manuscript.

Data Availability Statement: All unmodified data can be downloaded from https://doi.org/10.5281/zenodo.7059834 (accessed on 1 September 2022).

Conflicts of Interest: The authors declare no conflict of interest.

References

1. Donnelly, C.; Greuell, W.; Andersson, J.; Gerten, D.; Pisacane, G.; Roudier, P.; Ludwig, F. Impacts of climate change on European hydrology at 1.5, 2 and 3 degrees mean global warming above preindustrial level. *Clim. Chang.* **2017**, *143*, 13–26. [CrossRef]
2. Sun, Q.; Miao, C.; Hanel, M.; Borthwick, A.G.L.; Duan, Q.; Ji, D.; Li, H. Global heat stress on health, wildfires, and agricultural crops under different levels of climate warming. *Environ. Int.* **2019**, *128*, 125–136. [CrossRef] [PubMed]
3. Armaroli, N.; Balzani, V. The future of energy supply: Challenges and opportunities. *Angew. Chem. Int. Ed.* **2007**, *46*, 52–66. [CrossRef] [PubMed]
4. Vos, J.G.; Kelly, J.M. Ruthenium polypyridyl chemistry; from basic research to applications and back again. *Dalton Trans.* **2006**, *41*, 4869–4883. [CrossRef] [PubMed]
5. Wang, M.; Na, Y.; Gorlov, M.; Sun, L. Light-driven hydrogen production catalysed by transition metal complexes in homogeneous systems. *Dalton Trans.* **2009**, *33*, 6458–6467. [CrossRef]
6. Goldsmith, J.I.; Hudson, W.R.; Lowry, M.S.; Anderson, T.H.; Bernhard, S.J. Discovery and high-throughput screening of heteroleptic iridium complexes for photoinduced hydrogen production. *Am. Chem. Soc.* **2005**, *127*, 7502–7510. [CrossRef]

7. Pfeffer, M.G.; Schäfer, B.; Smolentsev, G.; Uhlig, J.; Nazarenko, E.; Guthmuller, J.; Kuhnt, C.; Wächtler, M.; Dietzek, B.; Sundström, V.; et al. Palladium versus platinum: The metal in the catalytic center of a molecular photocatalyst determines the mechanism of the hydrogen production with visible light. *Angew. Chem. Int. Ed.* **2015**, *54*, 5044–5048. [CrossRef]

8. Lämmle, M.; Pilz, T.D.; Kutta, R.J.; Müßler, M.; Mengele, A.K.; Görls, H.; Heinemann, F.W.; Rau, S. Insights into the different mechanistic stages of light-induced hydrogen evolution of a 5, 5′-bisphenanthroline linked RuPt complex. *Dalton Trans.* **2022**. [CrossRef]

9. Mengele, A.K.; Kaufhold, S.; Streb, C.; Rau, S. Generation of a stable supramolecular hydrogen evolving photocatalyst by alteration of the catalytic center. *Dalton Trans.* **2016**, *45*, 6612–6618. [CrossRef]

10. Ozawa, H.; Kobayashi, M.; Balan, B.; Masaoka, S.; Sakai, K. Photo-Hydrogen-Evolving Molecular Catalysts Consisting of Polypyridyl Ruthenium (II) Photosensitizers and Platinum (II) Catalysts: Insights into the Reaction Mechanism. *Chem. Asian J.* **2010**, *5*, 1860–1869. [CrossRef]

11. Ozawa, H.; Haga, M.A.; Sakai, K.J. A photo-hydrogen-evolving molecular device driving visible-light-induced EDTA-reduction of water into molecular hydrogen. *Am. Chem. Soc.* **2006**, *128*, 4926–4927. [CrossRef] [PubMed]

12. Pfeffer, M.G.; Kowacs, T.; Wächtler, M.; Guthmuller, J.; Dietzek, B.; Vos, J.G.; Rau, S. Optimization of hydrogen-evolving photochemical molecular devices. *Angew. Chem. I. Edt.* **2015**, *54*, 6627–6631. [CrossRef] [PubMed]

13. Ozawa, H.; Yokoyama, Y.; Haga, M.-A.; Sakai, K.J. Syntheses, characterization, and photo-hydrogen-evolving properties of tris(2,2′-bipyridine)ruthenium(ii) derivatives tethered to a cis-Pt(ii)Cl2 unit: Insights into the structure–activity relationship. *Chem. Soc. Dalton Trans.* **2006**, *12*, 1197–1206. [CrossRef] [PubMed]

14. Zhang, P.; Wang, M.; Li, X.Q.; Cui, H.G.; Dong, J.F.; Sun, L.C. Photochemical hydrogen production with molecular devices comprising a zinc porphyrin and a cobaloxime catalyst. *Sci. China Chem.* **2012**, *55*, 1274–1282. [CrossRef]

15. Li, C.; Wang, M.; Pan, J.; Zhang, P.; Zhang, R.; Sun, L.J. Photochemical hydrogen production catalyzed by polypyridyl ruthenium– cobaloxime heterobinuclear complexes with different bridges. *Organomet. Chem.* **2009**, *694*, 2814–2819. [CrossRef]

16. Petermann, L.; Staehle, R.; Pfeifer, M.; Reichardt, C.; Sorsche, D.; Wächtler, M.; Popp, J.; Dietzek, B.; Rau, S. Oxygen-Dependent Photocatalytic Water Reduction with a Ruthenium (imidazolium) Chromophore and a Cobaloxime Catalyst. *Chem. Eur. J.* **2016**, *22*, 8240–8253. [CrossRef]

17. Karnahl, M.; Kuhnt, C.; Ma, F.; Yartsev, A.; Schmitt, M.; Dietzek, B.; Rau, S.; Popp, J. Tuning of photocatalytic hydrogen production and photoinduced intramolecular electron transfer rates by regioselective bridging ligand substitution. *ChemPhysChem* **2011**, *12*, 2101–2109. [CrossRef]

18. Zedler, L.; Wintergerst, P.; Mengele, A.K.; Müller, C.; Li, C.; Dietzek-Ivanšić, B.; Rau, S. Outpacing conventional nicotinamide hydrogenation catalysis by a strongly communicating heterodinuclear photocatalyst. *Nat. Commun.* **2022**, *13*, 2538. [CrossRef]

19. Yamazaki, Y.; Takeda, H.; Ishitani, O.J. Photocatalytic reduction of CO2 using metal complexes. *Photochem. Photobiol. C* **2015**, *25*, 106–137. [CrossRef]

20. Lei, P.; Hedlund, M.; Lomoth, R.; Rensmo, H.; Johansson, O.; Hammarström, L.J. The role of colloid formation in the photoinduced H2 production with a RuII-PdII supramolecular complex: A study by GC, XPS, and TEM. *Am. Chem. Soc.* **2008**, *130*, 26–27. [CrossRef]

21. Pfeffer, M.G.; Müller, C.; Kastl, E.T.E.; Mengele, A.K.; Bagemihl, B.; Fauth, S.S.; Habermehl, J.; Petermann, L.; Wächtler, M.; Schulz, M.; et al. Active repair of a dinuclear photocatalyst for visible-light-driven hydrogen production. *Nat. Chem.* **2022**, *14*, 500–506. [CrossRef] [PubMed]

22. Griffiths, P.M.; Loiseau, F.; Puntoriero, F.; Serroni, S.; Campagna, S. New luminescent and redox-active homometallic dinuclear iridium (iii), ruthenium (ii) and osmium (ii) complexes prepared by metal-catalyzed coupling reactions Electronic supplementary information (ESI) available: Spectral data for 1–4, cyclic voltammogram for 3 and absorption and emission spectra for 1–3. *Chem. Commun.* **2000**, *23*, 2297–2298.

23. Gong, Z.J.; Narayana, Y.S.L.V.; Lin, Y.-C.; Huang, W.-H.; Su, W.-N.; Li, Y.-P.; Higuchi, M.; Yu, W.-Y. Rational synthesis of ruthenium-based metallo-supramolecular polymers as heterogeneous catalysts for catalytic transfer hydrogenation of carbonyl compounds. *Appl. Catal. B Environ.* **2022**, *312*, 121383. [CrossRef]

24. Stumper, A.; Pilz, T.D.; Schaub, M.; Görls, H.; Sorsche, D.; Peuntinger, K.; Guldi, D.; Rau, S. Efficient Access to 5-Bromo-and 5, 6-Dibromophenanthroline Ligands. *Eur. J. Inorg. Chem.* **2017**, *32*, 3799–3810. [CrossRef]

25. Rau, S.; Schäfer, B.; Grüßing, A.; Schebesta, S.; Lamm, K.; Vieth, J.; Görls, H.; Walther, D.; Rudolph, M.; Grummt, U.W.; et al. Efficient synthesis of ruthenium complexes of the type (R-bpy) 2RuCl2 and [(R-bpy) 2Ru (L–L)] Cl2 by microwave-activated reactions (R: H, Me, tert-But) (L–L: Substituted bibenzimidazoles, bipyrimidine, and phenanthroline). *Inorg. Chim. Acta* **2004**, *357*, 4496–4503. [CrossRef]

26. Wu, T.; Liu, J.; Liu, M.; Liu, S.; Zhao, S.; Tian, R.; Wei, D.; Liu, Y.; Zhao, Y.; Xiao, H.; et al. A nanobody-conjugated DNA nanoplatform for targeted platinum-drug delivery. *Angew. Chem. Int. Ed.* **2019**, *58*, 14224–14228. [CrossRef] [PubMed]

27. Suzuki, K.; Kobayashi, A.; Kaneko, S.; Takehira, K.; Yoshihara, T.; Ishida, H.; Shiina, Y.; Oishi, S.; Tobita, S. Reevaluation of absolute luminescence quantum yields of standard solutions using a spectrometer with an integrating sphere and a back-thinned CCD detector. *Phys. Chem. Chem. Phys.* **2009**, *11*, 9850–9860. [CrossRef]

28. Hossain, M.D.; Higuchi, M. Synthesis of metallo-supramolecular polymers using 5, 5′-linked bis (1, 10-phenanthroline) ligands. *Synthesis* **2013**, *45*, 753–758.

29. Yang, W.; Nakano, T. Synthesis of poly (1, 10-phenanthroline-5, 6-diyl) s having a π-stacked, helical conformation. *Chem. Commun.* **2015**, *51*, 17269–17272. [CrossRef]

30. Hu, Y.Z.; Xiang, Q.; Thummel, R.P. Bi-1, 10-phenanthrolines and their mononuclear Ru (II) complexes. *Inorg. Chem.* **2002**, *41*, 3423–3428. [CrossRef]

31. Rau, S.; Schäfer, B.; Gleich, D.; Anders, E.; Rudolph, M.; Friedrich, M.; Görls, H.; Henry, W.; Vos, J.G. A supramolecular photocatalyst for the production of hydrogen and the selective hydrogenation of tolane. *Angew. Chem. Int. Ed.* **2006**, *45*, 6215–6218. [CrossRef] [PubMed]

32. Karnahl, M.; Tschierlei, S.; Kuhnt, C.; Dietzek, B.; Schmitt, M.; Popp, J.; Schwalbe, M.; Krieck, S.; Görls, H.; Heinemann, F.W.; et al. Synthesis and characterization of regioselective substituted tetrapyridophenazine ligands and their Ru (II) complexes. *Dalton Trans.* **2010**, *39*, 2359–2370. [CrossRef]

33. Toyota, S.; Goto, A.; Kaneko, K.; Umetani, T. Syntheses, spectroscopic properties, and Cu (I) complexes of all possible symmetric Bi-1, 10-phenanthrolines. *Heterocycles* **2005**, *65*, 551–562. [CrossRef]

34. Juris, A.; Balzani, V.; Barigelletti, F.; Campagna, S.; Belser, P.; von Zelewsky, A. Ru (II) polypyridine complexes: Photophysics, photochemistry, eletrochemistry, and chemiluminescence. *Coord. Chem. Rev.* **1988**, *84*, 85–277. [CrossRef]

35. Barker, N.M.; Li, Y.X.; Lee, M.M.; Shen, C.R.; Krause, J.A.; Sun, S.S.; Lu, N.; Connick, W.B.; McMillin, D.R. Synthesis, Luminescence, and Structure of a Polymorphic Polyfluorinated Diiodoplatinum (II) Diimine Complex. *Inorg. Chem.* **2019**, *58*, 10716–10724. [CrossRef] [PubMed]

36. Ivanov, M.A.; Puzyk, M.V.; Balashev, K.P. Spectroscopic and electrochemical properties of dichlorodiimine complexes of Au (III) and Pt (II) with 1, 4-diazine derivatives of o-phenanthroline. *Russ. J. Gen. Chem.* **2006**, *76*, 843–848. [CrossRef]

37. Schwalbe, M.; Schäfer, B.; Görls, H.; Rau, S.; Tschierlei, S.; Schmitt, M.; Popp, J.; Vaughan, G.; Henry, W.; Vos, J.G. Synthesis and characterization of poly(bipyridine)ruthenium complexes as building blocks for heterosupramolecular arrays. *Eur. J. Inorg. Chem.* **2008**, *3*, 3310–3319. [CrossRef]

38. Petermann, L.; Staehle, R.; Pilz, T.D.; Sorsche, D.; Görls, H.; Rau, S. Synthetic Strategies for Variably Substituted Ruthenium–Imidazophenanthrolinium Complexes. *Eur. J. Inorg. Chem.* **2015**, *2015*, 750–762. [CrossRef]

39. Staehle, R.; Reichardt, C.; Popp, J.; Sorsche, D.; Petermann, L.; Kastner, K.; Streb, C.; Dietzek, B.; Rau, S. Ruthenium Imidazophenanthrolinium Complexes with Prolonged Excited-State Lifetimes. *Eur. J. Inorg. Chem.* **2015**, *2015*, 3932–3939. [CrossRef]

40. Schäfer, B.; Görls, H.; Meyer, S.; Henry, W.; Vos, J.G.; Rau, S. Synthesis and Properties of Tetrasubstituted 1, 10-Phenanthrolines and Their Ruthenium Complexes. *Eur. J. Inorg. Chem.* **2007**, *2007*, 4056–4063. [CrossRef]

41. Robin, M.B.; Day, P. Mixed valence chemistry—A survey and classification. *Adv. Inorg. Chem. Radiochem.* **1968**, *10*, 247–422.

42. Mengele, A.K.; Müller, C.; Nauroozi, D.; Kupfer, S.; Dietzek, B.; Rau, S. Molecular scylla and charybdis: Maneuvering between pH sensitivity and excited-state localization in ruthenium bi (benz) imidazole complexes. *Inorg. Chem.* **2020**, *59*, 12097–12110. [CrossRef] [PubMed]

43. Kamath, S.S.; Uma, V.; Srivastava, T.S. Experimental and quantum-chemical studies of 1H, 13C and 15N NMR coordination shifts in Pd (II) and Pt (II) chloride complexes with methyl and phenyl derivatives of 2, 2′-bipyridine and 1, 10-phenanthroline. *Inorg. Chim. Acta* **1989**, *161*, 49–56. [CrossRef]

44. Pavlishchuk, V.V.; Addison, A.W. Conversion constants for redox potentials measured versus different reference electrodes in acetonitrile solutions at 25 °C. *Inorg. Chim. Acta* **2000**, *298*, 97–102. [CrossRef]

45. Fraser, C.; Bosnich, B. Bimetallic reactivity. Investigation of metal-metal interaction in complexes of a chiral macrocyclic binucleating ligand bearing 6-and 4-coordinate sites. *Inorg. Chem.* **1994**, *33*, 338–346. [CrossRef]

46. Matsumoto, K.; Sakai, K. Structures and reactivities of platinum-blues and the related amidate-bridged platinumIII compounds. *Adv. Inorg. Chem.* **1999**, *49*, 375–427.

47. Sakai, K.; Ozawa, H. Homogeneous catalysis of platinum (II) complexes in photochemical hydrogen production from water. *Coord. Chem. Rev.* **2007**, *251*, 2753–2766. [CrossRef]

48. Kobayashi, M.; Masaoka, S.; Sakai, K. Synthesis, crystal structure, solution and spectroscopic properties, and hydrogen-evolving activity of [K (18-crown-6)] [Pt (ii) (2-phenylpyridinato) Cl 2]. *Photochem. Photobiol. Sci.* **2009**, *8*, 196–203. [CrossRef]

49. Chernyshev, V.M.; Astakhov, A.V.; Chikunov, I.E.; Tyurin, R.V.; Eremin, D.B.; Ranny, G.S.; Khrustalev, V.N.; Ananikov, V.P. Pd and Pt catalyst poisoning in the study of reaction mechanisms: What does the mercury test mean for catalysis? *ACS Catal.* **2019**, *9*, 2984–2995. [CrossRef]

50. Artero, V.; Fontecave, M. Solar fuels generation and molecular systems: Is it homogeneous or heterogeneous catalysis? *Chem. Soc. Rev.* **2013**, *42*, 2338–2356. [CrossRef]

51. Knoll, J.D.; Arachchige, S.M.; Brewer, K.J. A structurally diverse RuII, PtII tetrametallic motif for photoinitiated electron collection and photocatalytic hydrogen production. *ChemSusChem* **2011**, *4*, 252–261. [CrossRef] [PubMed]

52. Okazaki, R.; Masaoka, S.; Sakai, K. Photo-hydrogen-evolving activity of chloro (terpyridine) platinum (II): A single-component molecular photocatalyst. *Dalton Trans.* **2009**, *31*, 6127–6133. [CrossRef] [PubMed]

53. Amthor, S.; Hernández-Castillo, D.; Maryasin, B.; Seeber, P.; Mengele, A.K.; Gräfe, S.; González, L.; Rau, S. Strong Ligand Stabilization Based on π-Extension in a Series of Ruthenium Terpyridine Water Oxidation Catalysts. *Chem. Eur. J.* **2021**, *27*, 16871–16878. [CrossRef] [PubMed]

54. Heiland, M.; De, R.; Rau, S.; Dietzek-Ivanšić, B.; Streb, C. Not that innocent–ammonium ions boost homogeneous light-driven hydrogen evolution. *Chem. Commun.* **2022**, *58*, 4603. [CrossRef] [PubMed]
55. Whang, D.R.; Park, S.Y. Rational Design of an Electron-Reservoir PtII Complex for Efficient Photocatalytic Hydrogen Production from Water. *ChemSusChem* **2015**, *8*, 3204–3207. [CrossRef]